Electric polarization properties of single bacteria measured with electrostatic force microscopy

Theoretical and practical studies of Dielectric constant of single bacteria and smaller elements

Daniel Esteban i Ferrer

UNIVERSITAT DE BARCELONA

Electric polarization properties of single bacteria measured with electrostatic force microscopy

Theoretical and practical studies of Dielectric constant of single bacteria and smaller elements

Daniel Esteban i Ferrer

Barcelona, September 2014

DOCTORAL THESIS

6 Theoretical methodology for single bacteria dielectric characterization

6.1 Abstract

There are complex geometries, such as the one treated in the present thesis, for which it is not possible to find an analytical theoretical expression for the electrostatic force acting on the measuring probe. In these cases, one has to restore to numerical computations of the forces. In this chapter I will describe the study I performed to find the best way to numerically calculate the electric forces for the problems investigated. In this study I went from the easiest geometries (e.g. sphere on a plane) to the more complex ones (similar to the real geometry), to find the right tradeoff between complexity and accuracy.

In this part of the study I received important and valuable inputs from Dr. Martin A. Edwards to whom I am indebted.

6.2 Introduction

In the present thesis we are interested in a system geometry composed by a probe and a conductive substrate where our biological samples (bacteria, nanoparticles and viruses), will lie. As have been exposed in section 3.3 of the present thesis the measurements will mainly be carried out with the help of an AFM to perform electric force measurements using conductive probes. They will go from small tip apex radius (< 10 nm) for nanoparticles or viruses to larger ones (> 100 nm) for bacteria. The latter are the ones mostly used in this thesis.

The axisymmetric probe will be approximated as a disc cantilever with a thickness (T), and a length (L_{cant}) and a tip attached symmetrically underneath of such cantilever. This tip will be approximated as a cone with an aperture angle (θ) and a height (H) truncated to a tangent sphere with a radius (R). The sample has to be modeled with a thickness (h) a length (L) and a dielectric permittivity (ε_r) and the substrate as a reference electrode (potential = 0 volts). The limits of the simulation are set to insulating edges. To avoid the influence of them in the final solution, a variable transformation that approximates the radial length away from the active region to be infinite is used. All the edges of the cantilever are set to 1 Volt (see *Figure 6.1*a for a scheme of the model). Note that we are assuming an axially symmetric geometry. Depending on the actual geometry of the experiment a two dimensional axial symmetric geometry (cylindrical geometry) with just radial (r) and z dimensions might be considered. In this case the only allowed probe movement is in z direction (approximation-retraction) from the substrate. This is enough for the force vs. distance curves but insufficient for a lateral resolution study. This case has the limitation of not being able to simulate the realistic asymmetric probe (with the tip at one end of the lever). On the other hand the benefit of this axial symmetry is a much easier simulation to model avoiding most of the meshing problems and computing problems that in a three-dimensional analysis one has to face (degenerated tetrahedrons and/or cavities).

A 3D model would be good for a more realistic geometry and for highly non-symmetric samples (were axial symmetry approximations are not possible), taking into account cantilever geometry, tip holder, and scaling up. The biggest difficulty is that this modeling in three dimension and the very high aspect ratio of the tip (nanometer range for tip apex vs. micrometer to millimeter range of the larger structures) is almost impossible to mesh and the physical geometry (tilting angles, cone and tip etching, real cantilever and tip holder geometry, etc.) is very hard to obtain. Although we describe below some 3D calculations, they are something that should still be considered as future perspectives ahead of the present thesis.

Since this problem does not have an analytical solution, the only way to check the accuracy of the numerical calculations is to perform simulations by changing the simulation parameters (infinite limits, better mesh refinements, etc.) in the simulation model until arriving to a convergent solution. Besides the computational power limitation there is a need to check the convergence in as much situations as possible (at least in the range of the experimental parameters) what requires a systematic study of the experiment.

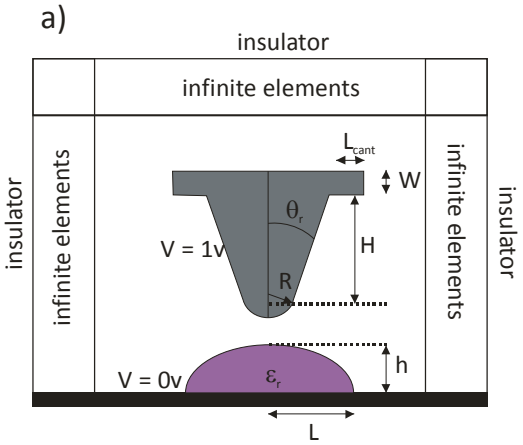

Figure 6.1 *Schematic representation of a truncated cone plus a tangent sphere and a cantilever (a) (not to scale). The figure also shows where the infinite elements are and the sample (a hemi-ellipsoid in this case).*

All of this gives an idea of the very high complexity and time consumption that accurate simulations can take. We have obtained additional, and valuable information, about the effects of the parameters on the simulations by analysing simpler problems for which an analytical solution is known and which bear some similarity with the problem at hand. With this objective in mind, I have performed a number of computations by assuming the probe can be modeled as a sphere.

In what follows I describe a number of models that have been analyzed in order to find the best numerical calculations conditions and to elucidate the effects of a number of geometric parameters into the calculated values.

The calculations presented in this chapter have been performed with the finite element numerical software COMSOL Multyphiscs® 3.4 (Comsol AB) running on a Pentium 4 dual core, with 4Gb RAM. The used solver was the direct Pardiso with default parameters unless otherwise stated. To run the scripts Matlab® LiveLink with Matlab® 2007 software were used. COMSOL is a commercial finite-element package that solves the Poisson's equation numerically by using a mesh to sub-divide the whole geometry (in partial differential equations). From these the expected forces on a probe are obtained as a function of the tip-sample separation, geometry and the electrical properties of the sample.

6.3 Sphere over infinite conductive substrate

As it has been said in the introduction of the section we have started by simulating a system with a known solution. There exist analytical solutions for the capacitance and electrostatic force of a sphere at a certain distance (z) from an infinite conductive substrate [35]. Here the numerical simulations for the approaching of the sphere to the surfaces are compared with the exact formula, in order to find the best meshing conditions for such problems.

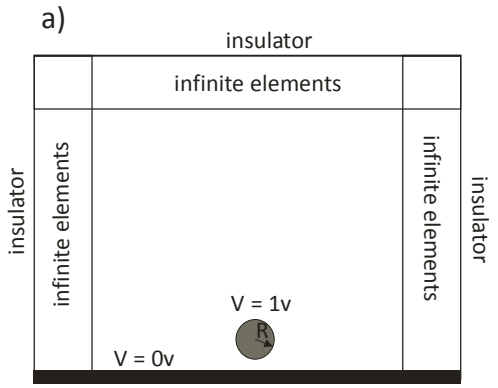

Figure 6.2 *(a) Model of a sphere over a substrate with its boundaries defined (not to scale).*

The sphere is a conductor and it is connected to the infinite conductive substrate (metal) at a certain AC potential. As it has been said in the introduction of this section the simulation area is approximated to infinite in the radial direction (r) from the sphere centre and in the positive z direction while the edges are set as electrical insulators (see Figure 6.2).

The sphere is set to an arbitrary 1 Volt and the substrate is set to 0 Volts (reference electrode). The exact formula from [35] gives us the capacitance of the system:

$$C_{metal}(R,z) = 4\pi\varepsilon_0 R \sum_{n=0}^{\infty} \frac{2\sqrt{\frac{z\left(2+\frac{z}{R}\right)}{R}}}{e^{(1+2n)\,cosh^{-1}\left(1+\frac{z}{R}\right)}-1} \qquad (6.1)$$

and the equation used to compare with the force simulations is

$$F_{metal} = \frac{1}{4}\frac{\partial C}{\partial z}V^2 \qquad (6.2)$$

from where

$$\frac{\partial C}{\partial z} = \frac{4}{V^2}F \qquad (6.3)$$

which is the magnitude that is going to be compared with the analytical formula, after derivation of Eq. (6.1).

After an extensive analysis of the presented case it has been elucidated that the most significant parameter to get accurate simulations is the refinement of the mesh in the edge of the sphere. A standard of quality to the simulation accuracy has been set to an error smaller than 5 % for the force analysis. To achieve this level of accuracy the maximum element size in the sphere edge has been found to be a twentieth of the sphere radius (i.e. 0.5 nm in the case of a 10 nm radius sphere). This refinement will be named fine mesh for the rest of the section, whereas the default meshing of the finite element software will be named coarse mesh.

The comparison of the real values (analytical formula) with the simulated ones for the capacitance gradient $\delta C/\delta z$ against the distance to the substrate (150 nm to 1.5 nm) for different radius (10 nm, 30 nm and 100 nm) can be seen in Figure 6.3a. The error percentage against the distance is also plotted for the 30 nm radius sphere in Figure 6.2b.

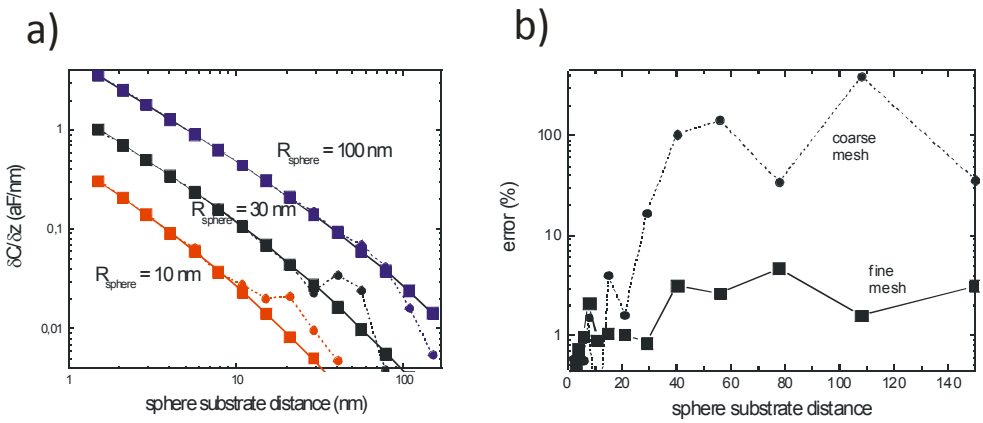

Figure 6.3 *(a) $\delta C/\delta z$ vs. distance curves for three different radius spheres (10 nm red, 30 nm black. Simulated values for a fine mesh on the sphere boundary (squares) and with a coarse mesh on the sphere boundary (circle and dashed line). The comparison with the analytical formula is given by the solid line. (b) Error percentage of the simulations compared to the analytical formula for the refined mesh (squares and solid line) and the coarse mesh (circles and dashed line) for the case of a 30 nm radius sphere.*

We clearly see that the refinement of the mesh on the edge of the sphere affects the results of the simulation to a big extent. While the coarse mesh give an error of up to 400 % in some points (circles and dashed line in Figure 6.3b the refined mesh shows a much smaller error where all the points lye below 3% of error (squares and solid line in Figure 6.3b).

6.4 Sphere over infinite length thick dielectric

A second model that has been analyzed is the case of a sphere over a laterally infinite insulator film on a metal. As the thickness of the bacteria is going to be in the order (and larger) of the tip radius it is interesting to see the effect of the dielectric thickness in the calculated electric forces.

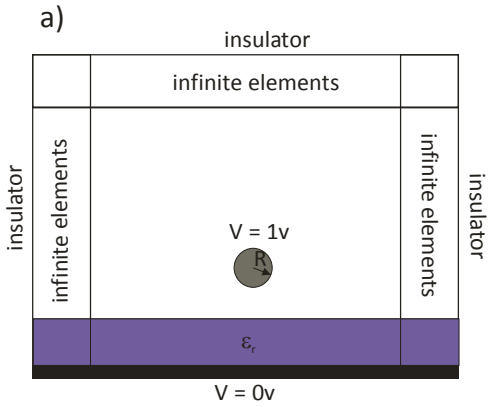

Figure 6.4 *(a) Model of a sphere over a thick dielectric with its boundaries defined (not to scale).*

In the model, the sphere is a conductor and it is connected to the infinite conductive substrate (metal) at 1 Volt with a dielectric infinite in the radial direction on top of the conductive substrate. The simulation area is approximated to infinite in the radial direction (r) from the sphere center and finite in the z direction. The edges are set as electrical insulators. For this problem, an analytical solution exists in the limit where the thickness of the dielectric tends to infinite [36]

$$C_{thick}(R, z, \varepsilon_r) = 4\pi\varepsilon_0 R \, sinh(\, cosh^{-1}(1 + \tfrac{z}{R})) \sum_{n=1}^{\infty} \left[(\tfrac{\varepsilon-1}{\varepsilon+1})^{n-1} \frac{1}{sinh(n \, cosh^{-1}(1+\frac{z}{R}))} \right]$$

(6.4)

which can be used to obtain the electric force acting on the sphere in this limit by using Eq. (6.2).

The first question that arises in this situation is finding the thickness of the substrate that makes the simulation to converge to the infinite thickness limit. In order to elucidate it, we have performed numerical calculations for different dielectric thicknesses and compared the results with the analytical formula. The thickness will be considered infinite when the calculated value with respect to the analytical formula is below a 3%. An example of the calculated values is shown in Figure 6.5 for the case of a substrate with a relative permittivity of 2 (which is the smaller value reported in biological samples) [28].

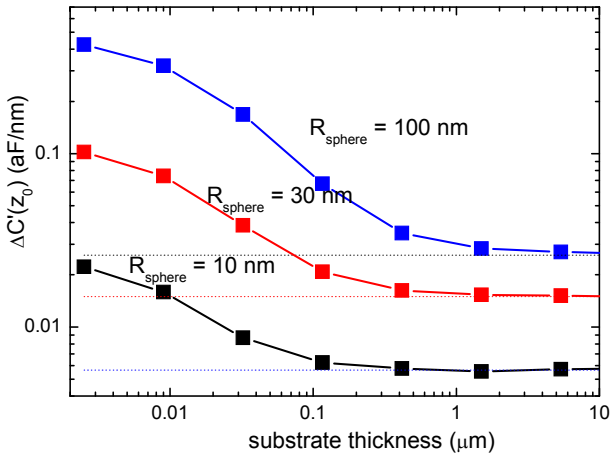

Figure 6.5 *Capacitance derivative difference vs. substrate thickness curves for three different radii of the sphere and at a fixed tip-substrate distance of 10 nm for a sphere of R = 100 nm black line, R= 30 nm red line and R= 10 nm blue line. The dotted line is the analytical limit when the substrate tends to infinite in the z direction for the three different radii. The reference distance is in all cases z_{ref}=150 nm.*

The tip substrate distance is fixed to z_0 = 10 nm (which is equal to a distance 10 + h nm over the metal electrode, where h is the sample

thickness) and calculations are done with respect to a reference point at a distance z_{ref} = 150 nm, which are about the distances used in the experimental part. Calculations for the capacitance gradient difference $\Delta C'(z_0)$ against the substrate thickness (2 nm to 10 μm) for different radius (10 nm, 30 nm and 100 nm) have been done (Figure 6.5).

We can see that the capacitance gradient decreases by increasing the film thickness until a saturation limit (different for each sphere radius) is reached. This limit can be seen to corresponds to the analytical formula presented in equation (6.4) represented with dot lines in Figure 6.5. We note that with the chosen simulation parameters, the error with the analytical formula in the infinitely thick limit is of less than a 3% as desired, meaning that the simulations are performing correctly in this case also.

We note that to achieve the infinite thickness limit the thickness of the substrate has to be thicker than around 20 times the radius of the sphere (i.e. 200 nm, 600nm and 2μm for the 10 nm, 30 nm and 100 nm radius spheres respectively). Also we verified, that the smaller the dielectric constant of the substrate the thicker it has to be to make the solution converge what gives us a minimum thickness for every substrates.

In the case of bacteria their height ranges from 200 nm to 700 nm which is not within the infinitely thick limit, and hence we would not be able to approximate them by an infinitely thick sample, and hence, analytical expressions of this type would not be useful.

6.5 Cone truncated to a tangent sphere over an infinite (length and height) dielectric

In the previous section the thickness of the substrate has shown to have an effect on the electric force acting on a sphere in close proximity to it for thicknesses well beyond the sphere radius. In this case, we show that also the probe geometry plays an important role in these problems. [30]. To this end we considered a cone truncated geometry as that shown in Figure 6.6. Finite element calculations were

used to calculate the force acting on the probe as a function of the substrate thickness and dielectric constant. Figure 6.7 reports $\Delta C'(z_0)$ at a near tip-sample distance, z_0 = 10 nm, as a function of the thickness h, for two reference distances, z_{ref} = 150 nm and 20 nm.

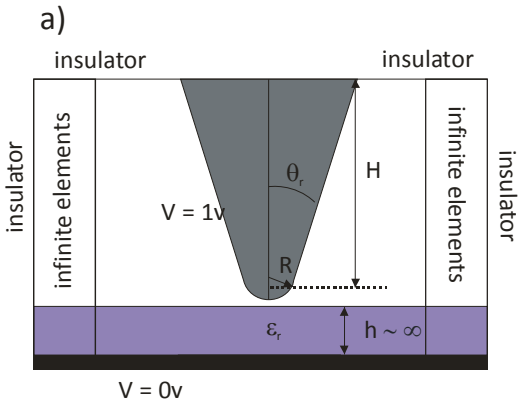

Figure 6.6 *(a) Model of a truncated cone + tangent sphere over a thick dielectric with its boundaries defined (not to scale).*

As for the case of the sphere results tend to become independent from the insulator thickness for large thicknesses. However, for the cone probe this happens at much larger distances, h > 100 μm (thick film limit), a value not certainly related to the tip radius but to the microscopic probe geometry. On the contrary when the thickness of the dielectric is between the thin (< 50 nm) and thick film limits, the film thickness matters and it has to be taken into account for quantitative comparisons (this will be the case for the bacteria studies). *Figure 6.8* shows the calculated $\Delta C'(z_0)$ as a function of the dielectric constant of the insulator in the thick film limit (h = 250 μm) overlaid with some experimental points obtained by Dr. L. Fumagalli [30]. The experimental results perfectly match the calculated values in this limit, thus additionally validating the numerical approach developed.

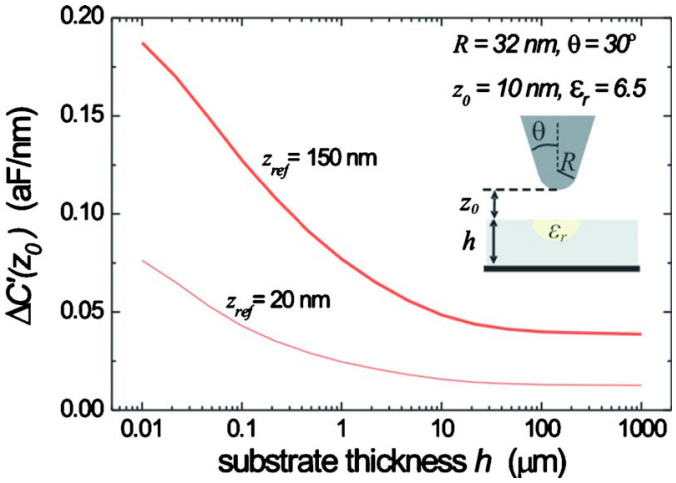

Figure 6.7 *Calculated $\Delta C'(z_0)$ as a function of the insulator thickness at tip-sample distance z_0 = 10 nm for ε_r = 6.5. Reference distances of: z_{ref} = 150 nm (thick line) and 20 nm (thin line).*

We note that by using the analytical model of a sphere on an infinite dielectric instead of simulating the whole probe would significantly under-estimate the dielectric constants and overestimate the tip radius calibration on metal (see dashed line in Figure 6.8).

We then conclude, that it is important to include the total cone height in the geometry as, despite the locality of the measurement, on a thick insulator the micrometric region of the upper cone can influence the shape of the electric field near the apex and the very lower part of the cone, leading to a systematic under-estimation of the dielectric constant if the whole cone is not included.

A similar effect was already discussed by Sacha and Sáenz [37] where the cantilever was considered as an infinite plane. A further refinement to the method shown here would require including the cantilever into the simulated model and the full three-dimensional simulation of the cantilever-probe system. An approximation of the cantilever addition effect has been recently proposed in our group (using axial symmetry) [38]. In the same article also the finite-size effects of a dielectric film had been taken into account.

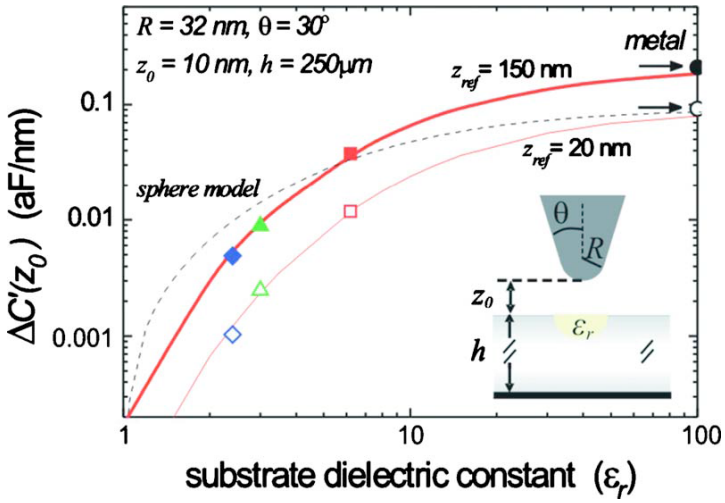

Figure 6.8 *Calculated $\Delta C'(z_0)$ as a function of the insulator dielectric constant at tip-sample distance z_0 = 10 nm for h = 250 μm. Two reference distances are considered: z_{ref} = 150 nm (thick line) and 20 nm (thin line). Some experimental data are shown for the two references (filled and unfilled symbols, respectively). The prediction of the analytical model of a sphere on an infinite dielectric is also shown dashed line for z_{ref} = 20 nm and radius 38 nm (radius chosen to fit the calibration measure).*

The first conclusion of this section is that in the ranges of the studied bacteria heights (200-700 nm) they cannot be considered infinitely thick, and hence the topography of each individual bacterium should be analyzed in order to achieve a quantitative modeling of the experiments. The second conclusion is that the spherical models are not suitable for a quantitative study of neither the tip radius calibration (metal substrate) nor the dielectric constant extraction. Hence, realistic tip models need to be used.

6.6 Cone truncated to a tangent sphere over an oblate spheroid

In addition to the probe geometry, also the sample geometry can play an important role in the calculations. We illustrate it in the present section by comparing the results obtained for a realistic bacterial shape (Figure 6.9) and a rectangular bacterial shape (Figure 6.10). In this case the probe geometry is a truncated cone of H = 15 μm, R = 300 nm and $\theta = 30^{o}$ over an oblate spheroid, representing the realistic bacteria shape (see Figure 6.9), and over a rectangular dielectric, representing the approximate bacteria shape (see Figure 6.12).

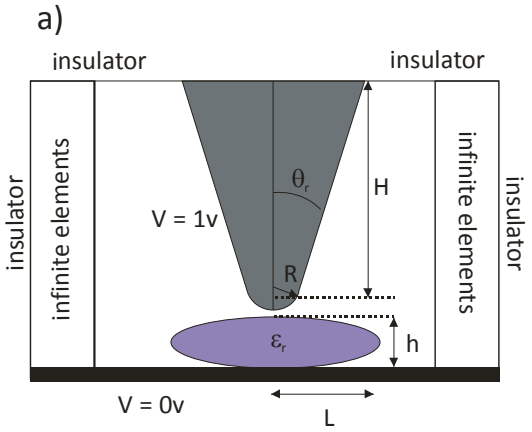

Figure 6.9 *(a) Model of a cone truncated to a tangent sphere over an oblate spheroid with its boundaries defined (not to scale).*

In Figure 6.11 the simulation of both geometries are plotted with h = 600 nm and L = 700 nm in both cases for ε_r = 3, 5 and 10. These values are chosen as being the worst case of the ranges obtained experimentally.

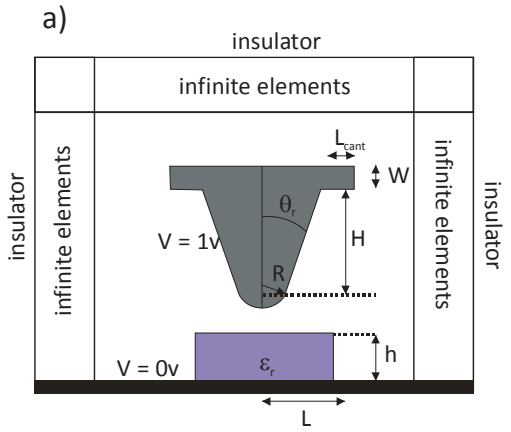

Figure 6.10 *(a) Model of a cone truncated to a tangent sphere over a thick dielectric with its boundaries defined (not to scale).*

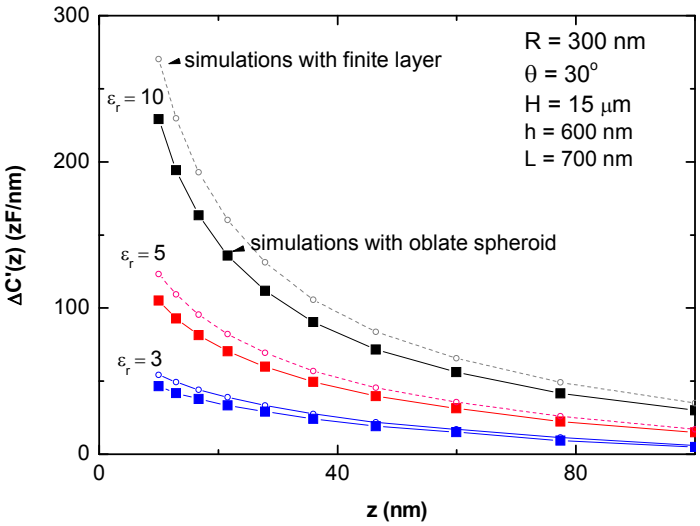

Figure 6.11 *Simulations of ΔC' (z) vs. distance to sample for a geometry using a finite dielectric layer (circles and dashed line) and using a dielectric oblate spheroid (squares and solid lines) for different permittivities 3, 5 and 10 (blue, red and black respectively). The simulation parameters are H = 15 mm, θ = 30°, R = 300 nm, L = 700 nm and h = 600 nm.*

The difference $\Delta C'$ (z) of the finite layer is higher as expected since the volume is larger and the upper part is closer to the tip apex. The error when using the finite layer instead of the oblate spheroid can be up to 18 % or even larger for bigger permittivities. The error percentage as a function of the proximity to the sample is shown in Figure 6.12. As expected the further from the sample the less its geometry affect the results.

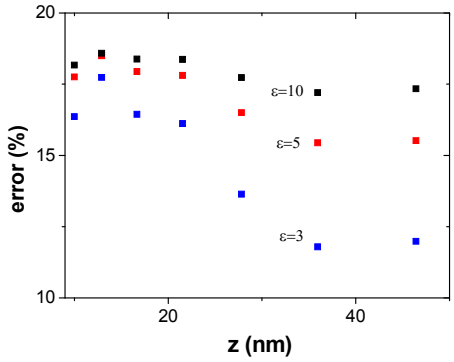

Figure 6.12 *The error percentage of $\Delta C'$ (z) using the finite dielectric layer instead of an oblate spheroid geometry vs. distance to sample.*

The conclusion is that if a shape different than a finite dielectric layer has to be studied (as is the case of bacteria) the simulated geometry has to be as close as it can be to the reality since the finite layer geometry is not a good approximation.

6.7 Cone truncated to a tangent sphere over an oblate hemi-spheroid

In the search for the more realistic geometry, we have considered also the case of modeling the bacteria as an oblate hemi-spheroid, since this could better represent the shape of an adsorbed bacterium. In this section the oblate hemi-spheroid will be compared with the oblate spheroid (previous geometry). A description of the geometry can be seen in Figure 6.13.

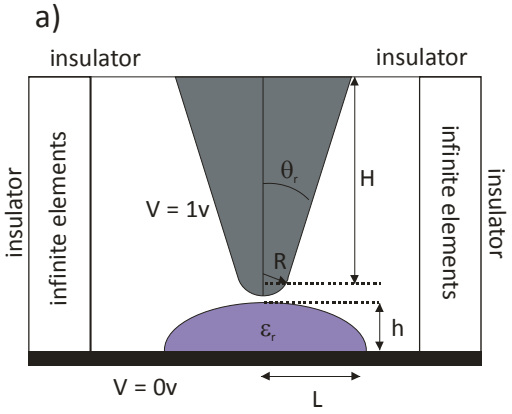

Figure 6.13 *(a) Model of a cone truncated to a tangent sphere over an oblate hemi-spheroid with its boundaries defined (not to scale).*

Comparing both geometries in simulations of approach curves to the sample with H = 15 μm, $\theta = 30^{o}$, R = 300 nm, h = 600 nm and L = 700 nm (worst case scenario of experimental ranges) the difference go up to 7.5 % in some cases (close to the sample and for high ε_r) (Figure 6.14). Although the difference is not enormous it is still significant so again an accurate topography of the sample will have an important role.

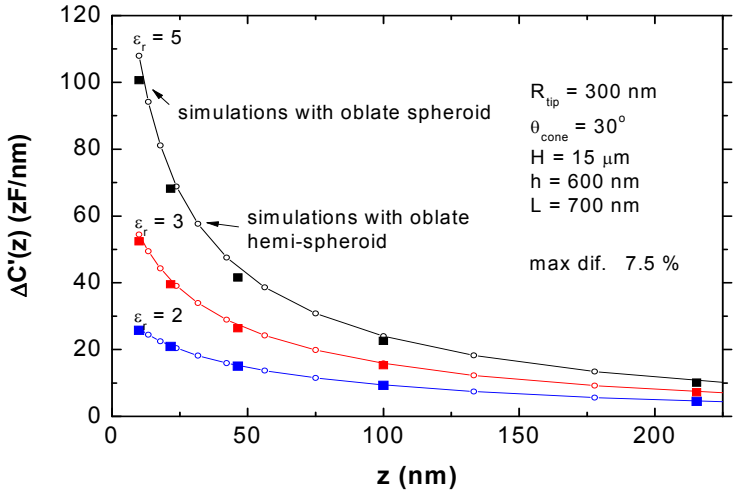

Figure 6.14 *Simulations of ΔC' (z) vs. distance to sample for a geometry using an oblate hemi-spheroid (circles and dashed line) and using a dielectric oblate spheroid (squares and solid lines) for different permittivities 2, 3 and 5 (blue, red and black respectively). The simulation parameters are H = 15 mm, θ = 30°, R = 300 nm, L = 700 nm and h=600 nm.*

6.8 Cone truncated to a tangent sphere over a tri-axial hemi-ellipsoid

As it has been commented 3D simulations are difficult to perform and some random configurations can lead to impossible meshes, besides higher errors due to coarser meshes in calculations (see ***Sphere over infinite conductive substrate***). We overcome these difficulties to an extent to enable us to assess the axisymmetric models to the more realistic non-axisymmetric model. The 3D model used in the comparison is shown in Figure 6.15.

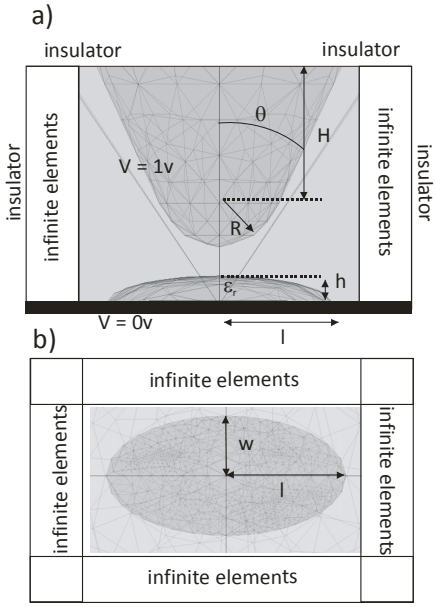

Figure 6.15 *Model of a cone truncated to a tangent sphere over a tri-axial hemi-ellipsoid with its boundaries defined (not to scale). (a) is the side view, whereas (b) is the top view.*

For calculations with the tip above the center of the sample, the oblate hemi spheroid geometry resulted in almost identical forces to the tri-axial ellipsoidal one (errors < 3%) as long as the polar axis, h, is maintained and the equatorial axis of the oblate hemispheroid, L, is taken so that the volume of the sample is preserved, i.e. $L = 1/2(l \cdot w)^{1/2}$, where l and w are the width and length, respectively. The results for L = 700 nm, l = 2 μm, w = 1 μm, h = 600 nm, R = 300 nm, H = 15 mm and q = 30^{o} (worst case scenario with experimental data) are shown in *Figure 6.16*.

A cone of H = 2μm would have suffice (without a cantilever) although the H = 15 mm have been used for consistency with the axial symmetric simulations. This fact, though, could be used for further full-3D studies of non-symmetric and/or non-homogeneous samples or probes making them simpler.

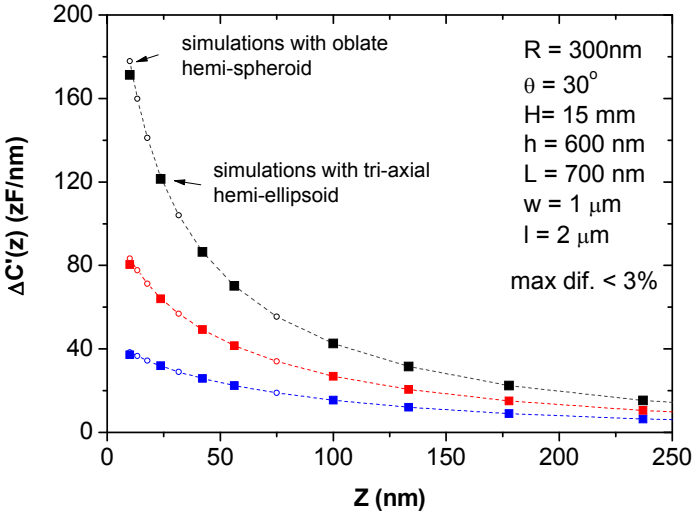

Figure 6.16 *Simulations of $\Delta C'(z)$ vs. distance to sample for a geometry using an oblate tri-axial hemi-ellipsoid (circles and dashed line) and using a dielectric oblate spheroid (squares and solid lines) for different permittivities 2, 3 and 5 (blue, red and black respectively). The simulation parameters are H = 15 mm, $\theta = 30^{o}$, R = 300 nm, L = 700 nm and h=600 nm.*

The results show that for the particular case of bacteria and as long as measurements are reduced to the bacteria center, an axisymmetric model can be used, which facilitates enormously its practical implementation.

6.9 Conclusions

For simplicity in mesh, accuracy and similarity to the realistic system (topography) the ***Cone truncated to a tangent sphere over symmetric hemi-ellipsoid*** has been chosen for the bacteria dielectric characterization. In the case of the validation of the technique on a silicon nitride pattern (see chapter 4) the model of the ***Cantilever plus cone truncated to a tangent sphere over a rectangular dielectric*** is used.